Effect of heat treatments on the microstructure and mechanical properties of a cast intermetallic Ti-44Al-4Nb-4Zr-0.2Si-0.3B alloy

J. Lapin[1]*, Z. Gabalcová[1], O. Bajana[1], D. Daloz[2]

[1] *Institute of Materials and Machine Mechanics, Slovak Academy of Sciences, Račianska 75, 831 02 Bratislava, Slovak Republic*
[2] *Ecole Nationale Supérieure des Mines de Nancy, LSG2M, Parc de Saurupt, F-54042 Nancy, Cedex, France*

Received 6 November 2006, received in revised form 5 December 2006, accepted 6 December 2006

Abstract

The effect of two types of heat treatment, (i) cyclic heat treatment composed of annealing at temperatures ranging from 1523 to 1623 K combined with oil quenching and (ii) heat treatment consisting of annealing at a constant annealing temperature of 1623 K combined with cooling at constant rates ranging from 0.056 to 1.181 $K \cdot s^{-1}$, on the microstructure and mechanical properties of a cast Ti-44Al-4Nb-4Zr-0.2Si-0.3B (at.%) alloy was studied. Grain size and Vickers hardness are decreased to final values after the first heat treatment cycle. Increasing number of the cycles has no statistical effect on these parameters. This heat treatment does not improve room-temperature tensile ductility. On the contrary, tensile tests at 1023 K showed clear yielding and plastic elongation before fracture ranging from 0.21 to 0.32 %. Increase of the cooling rate decreases mean interlamellar α_2-α_2 spacing within lamellar $\alpha_2 + \gamma$ grains and leads to formation of numerous equiaxed β(B2), γ and ω grains in the microstructure. Vickers hardness, room-temperature compressive yield stress, high-temperature tensile yield stress and high-temperature ultimate tensile stress increase with increasing cooling rate. Change of the cooling rate does not improve room-temperature ductility.

K e y w o r d s: titanium aluminides, TiAl, heat treatment, microstructure, mechanical properties

1. Introduction

Intermetallic alloys based on γ-TiAl have been extensively studied for various high-temperature structural applications [1–6] in the aerospace and automotive industries. They exhibit lower density when compared to nickel-based superalloys [7–9], nickel [10–12] or iron [13–15] based intermetallic alloys and higher creep strength, tensile strength and oxidation resistance than conventional titanium alloys at higher temperatures [16, 17]. Among various processing routes, precise casting is an economical way for the production of these alloys and relevant components [18]. However, main disadvantages of cast TiAl based alloys still remain low room temperature ductility, fracture toughness, large scatter of mechanical properties of coarse grained material and low creep resistance at temperatures higher than about 1073 K. As shown previously for forged material [19], fine-grained microstructure leads to higher room-temperature ductility and improved deformability of these alloys at higher temperatures. There are two approaches to refine the microstructure of cast TiAl based alloys: (i) through solidification by affecting alloy composition and (ii) through solid state transformations by appropriate heat treatments and thermomechanical processing. Alloying by boron was identified to be very effective and economical way to refine grain structure of cast alloys. A minimum amount of boron to achieve grain refinement was identified to be about 0.5 at.% [20, 21]. Below this level, little or no impact on the grain size is obtained whereas adding larger amounts of boron does not reduce the grain size further [22]. Amount of boron ranging from 0.2 to 1 at.% promotes formation of lamellar microstructure [23], suppresses formation of feathery and massive

*Corresponding author: tel.: +421 2 49268290; fax: +421 2 44253301; e-mail address: ummslapi@savba.sk

γ-TiAl [24] and hinders uncontrolled grain growth during heat treatments [20]. Among various boron doped alloys, alloy with nominal composition Ti-44Al-4Nb-4Zr-0.2Si-0.3B (at.%) was developed with the aim to improve creep resistance [22]. In this alloy, both boron and silicon refine the microstructure and improve creep resistance. Addition of zirconium stabilizes β phase (Ti-based solution with cubic crystal structure) in the microstructure and increases creep resistance by solid solution strengthening. Niobium stabilizes β phase and promotes formation of $\gamma + \beta$ duplex type of microstructure during heat treatments.

The aim of this paper is to study the effect of heat treatments on the microstructure and mechanical properties of a cast Ti-44Al-4Nb-4Zr-0.2Si-0.3B (at.%) alloy. The grain size, interlamellar spacing, hardness, tensile and compression properties are reported and discussed.

2. Experimental procedure

The studied alloy with nominal chemical composition Ti-44Al-4Nb-4Zr-0.2Si-0.3B (at.%) alloy was prepared by vacuum arc remelting in the form of cylindrical ingot with a diameter of 90 mm and length of 400 mm. Ingots for heat treatments and mechanical testing with dimensions of 10 × 20 × 70 mm were cut in the vicinity of central part of the as-cast ingot by electro-spark machining. After cutting, the ingots were solution annealed at a temperature of 1623 K for 1 h in a dynamic argon atmosphere and then quenched into oil at a cooling rate of 80 $K \cdot s^{-1}$. During solution annealing and quenching, the temperature of the ingots was continuously measured by PtRh30–PtRh6 thermocouple.

Two types of heat treatments were performed: (i) cyclic heat treatment combined with oil quenching and (ii) heat treatment combined with cooling at various constant cooling rates. For the cyclic heat treatments, six annealing temperatures ranging from 1523 to 1623 K were used. One heat treatment cycle consisted of heating of ingots to the annealing temperature at a heating rate of 2.167 $K \cdot s^{-1}$, dwell at this temperature for 600 s and then quenching into oil. The number of repeated cycles was selected to be 1, 3, 5 and 7. The heat treatment was performed in a dynamic argon atmosphere. After the cyclic heat treatment the specimens were subjected to stabilization annealing at 1173 K for 6 h and furnace cooling to room temperature under argon atmosphere. The heat treatment combined with cooling at constant cooling rates consisted of heating of ingots to an annealing temperature of 1623 K at a heating rate of 2.167 $K \cdot s^{-1}$, dwell at this temperature for 600 s and cooling at constant cooling rates selected in a range from 0.056 to 1.181 $K \cdot s^{-1}$ to a temperature of 1073 K. The heat treatment was finalized by air cooling to room temperature.

For each studied heat treatment conditions, five flat tensile specimens with the gauge dimensions 4 × 6 mm and gauge length of 30 mm were prepared by electro-spark machining. In order to avoid surface effects on mechanical properties, each gauge section of the specimens was carefully grinded and mechanically polished using diamond paste (1 μm grain size). Tensile tests were conducted at 293 and 1023 K at an initial strain rate of 1×10^{-3} s^{-1}. The offset tensile yield strength was measured at 0.2% plastic strain and the ductility was evaluated from the total plastic elongation to fracture. Compression specimens with dimensions 4 × 4 × 7 mm were prepared by electro-spark machining followed by grinding and mechanical polishing using diamond paste. Room-temperature compression tests were performed at an initial strain rate of 1×10^{-4} s^{-1}. The offset compressive yield strength was measured at 0.2% plastic strain. Both the tensile and compression tests were conducted on computer controlled screw-driven Zwick machine in air. Vickers hardness measurements were performed at an applied load of 296 N.

Microstructural analysis was performed by light optical microscopy (LOM) and scanning electron microscopy (SEM). LOM and SEM samples were prepared using standard metallographic techniques and etched in a reagent of 50 ml H_2O, 3 ml HNO_3 and 1.5 ml HF. Grain size and interlamellar spacing were measured by linear intercept method using computerized image analyzer.

3. Results and discussion

3.1. Microstructure

Figure 1 shows the typical geometry and microstructure of the as-cast ingots used for the heat treatments and mechanical testing. The ingot contains two different regions designated as A and B with different grain size, as illustrated in Fig. 1a. Figure 1b shows the typical microstructure of equiaxed grains observed in both regions. The mean grain size was measured to be 50 μm and 61 μm in the edge (region A) and central (region B) parts of the ingot, respectively. Due to non-homogenous distribution of equiaxed grain and some chemical heterogeneity, each ingot was solution annealed in $\alpha+\beta$ phase region (α and β phases are Ti-based solid solutions with hexagonal and cubic crystal structure, respectively) at a temperature of 1623 K for 1 h and then quenched into the oil. Such heat treatment resulted in a homogenous grain size distribution in the ingots connected with a decrease of mean grain size to 44 μm.

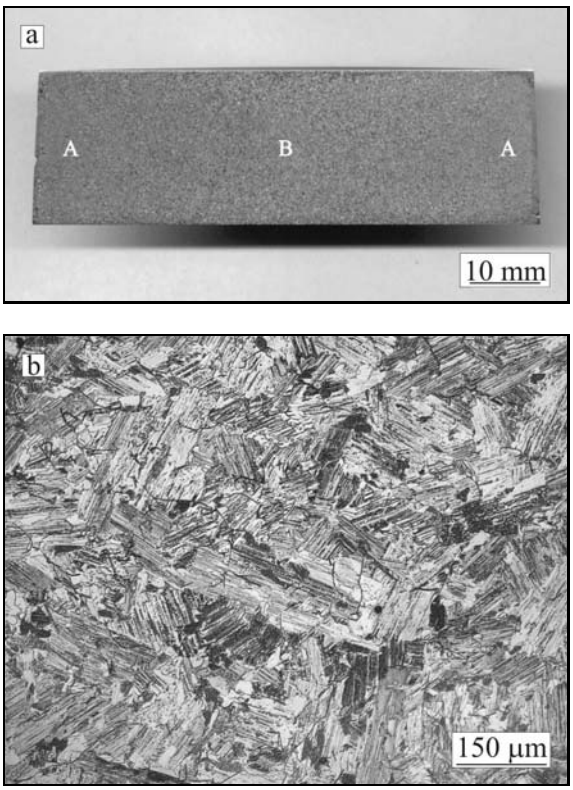

Fig. 1. The typical geometry and microstructure of ingots before heat treatments: (a) typical geometry of the ingot with marked regions A and B; (b) microstructure of equiaxed grains.

3.1.1. Effect of cyclic heat treatment on the microstructure

Figure 2 shows the typical microstructure of the studied alloy after quenching from three annealing temperatures of 1543, 1563 and 1593 K. The microstructure of ingots quenched from a temperature of 1593 K consists of lamellar grains composed of $\alpha_2(Ti_3Al)$ and γ(TiAl) lamellae and the mixture of β, γ and ω (Ti-based solid solution with $B8_2$ hexagonal crystal structure) grains, which are formed at lamellar grain boundaries and triple junctions, as seen in Fig. 2a. It should be noted that the β phase transforms at relatively high temperatures (above 1373 K) to the ordered B2 phase. Since it is not possible to distinguish β from B2 by the applied metallographic techniques, only simple designation of the β(B2) phase is used in this work. As reported by Cheng and Willis [25], the annealing temperature of 1593 K corresponds to a minimum temperature for the stability of the $\alpha+\beta$ phase region. The γ grains observed in the microstructure are formed during stabilization annealing at 1173 K due to the decomposition of the β(B2) phase. However, the β phase is not stable during cooling to room temperature and further transforms to ω phase

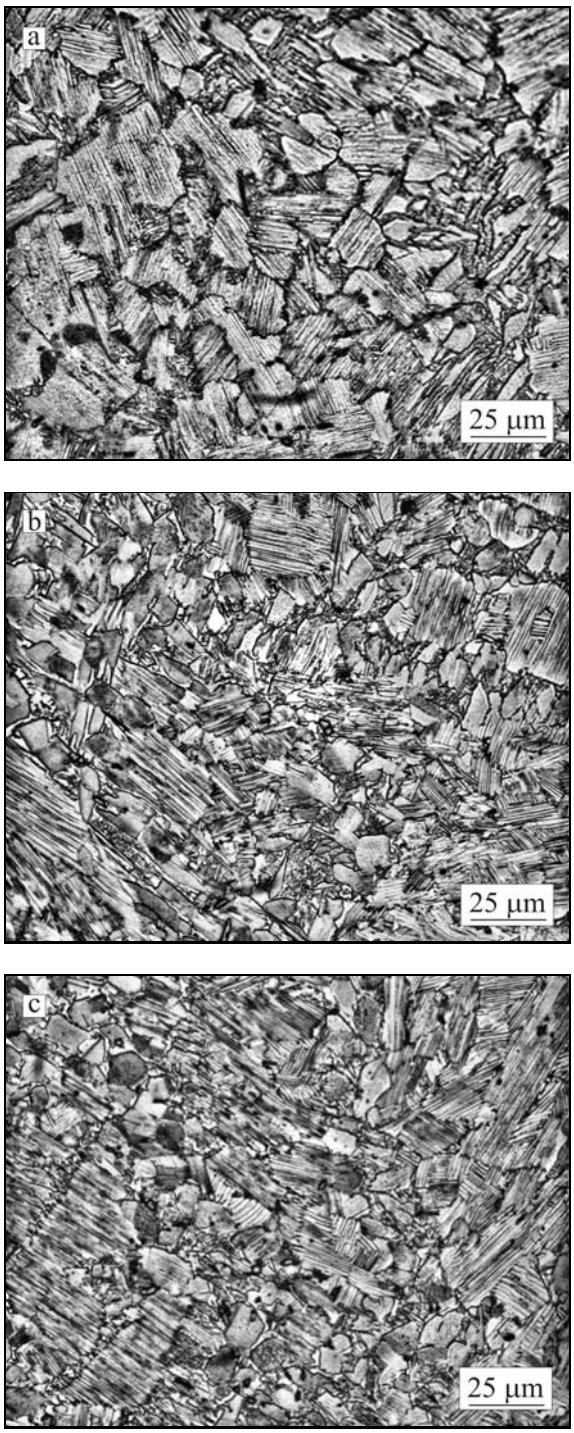

Fig. 2. LOM micrographs showing the effect of annealing temperature on the microstructure of the ingots after 1 cycle of the cyclic heat treatment and stabilization annealing at 1173 K for 6 h. Annealing temperatures: (a) 1593 K; (b) 1563 K; (c) 1543 K.

[25, 26]. Figure 2b shows the typical microstructure of the ingots annealed at 1563 K and aged at 1173 K for 6 h. The microstructure consists of equiaxed β(B2), γ, ω and lamellar $\alpha_2+\gamma$ grains. The annealing tempera-

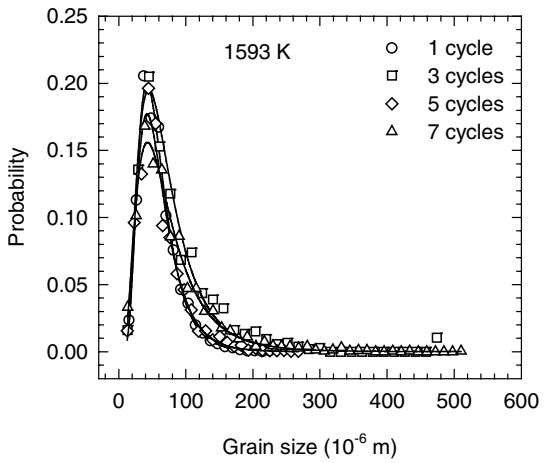

Fig. 3. Log-normal distribution curves of measured grain size for ingots annealed at 1593 K and oil quenched. The number of heat treatment cycles is indicated in the figure.

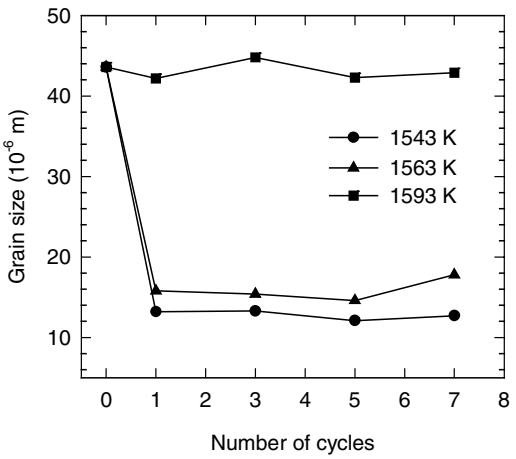

Fig. 4. Dependence of mean grain size on the number of heat treatment cycles. The annealing temperatures of the cyclic heat treatment are indicated in the figure.

ture of 1563 K is a minimum temperature for stability of three phase regions composed of $\alpha + \beta + \gamma$ phases [25]. Figure 2c shows the typical microstructure of the ingots annealed at 1543 K and aged at 1173 K for 6 h. The microstructure consists of equiaxed lamellar $\alpha_2+\gamma$, β(B2), γ and ω grains and is similar to that obtained after quenching from 1563 K. The temperature of 1543 K corresponds to a minimum temperature for the stability of two-phase $\alpha + \gamma$ region [25]. Below this temperature, three-phase microstructure composed of $\alpha + \mathrm{B2} + \gamma$ was reported to be stable during annealing [25].

Statistical analysis of the measured grain size data showed that the best fit can be achieved by a log-normal distribution function. Figure 3 shows examples of log-normal distribution curves for the ingots quenched from the annealing temperature of 1593 K. The correlation coefficients of these fits r^2 were determined to be better than 0.96. Similar distribution curves were determined for all cyclic heat treatment conditions. Figure 4 summarizes the effect of number cycles on mean grain size for all heat treated ingots. It is clear from this figure that the annealing at 1593 K combined with quenching has no statistical effect on the mean grain size when compared to the grain size before heat treatments. However, lower annealing temperatures of 1543 and 1563 K result in a significant grain size reduction. Finer grain microstructure is achieved after the first cycle and further increase of number of cycles has no statistical effect on the mean grain size. As shown recently by Wang et al. [27], cyclic heat treatment is an effective method to refine microstructure of alloys, which exhibit massive transformations of α to γ phase during quenching. However, the microstructure observations of the as-quenched ingots of the studied alloy showed no massive transformation of α to γ phase during oil quenching. These experimental observations are in good agreement with proposed continuous cooling transformation (CCT) diagram suggested by Cheng and Loretto [26] for a boron-free Ti-44Al-4Nb-4Zr-0.2Si (at.%) alloy where no massive transformation is expected.

3.1.2. Effect of cooling rate on the microstructure

Figure 5 shows the typical microstructure of the ingots after cooling from an annealing temperature of 1623 K at constant cooling rates. The selected annealing temperature corresponds to the stability of $\alpha + \beta$ phases in the microstructure of the studied alloy [25]. Figure 5a shows that relatively large lamellar $\alpha_2 + \gamma$ grains remain in the microstructure and fine grains of β(B2), and so-called transformed β composed of γ and ω phases is formed at the grain boundaries after cooling at the highest rate of 1.181 $\mathrm{K \cdot s^{-1}}$. This heat treatment results in a mean grain size of 59 μm, which is higher than that of 44 μm measured after cyclic heat treatments (see Fig. 4). Intermediate cooling rates are found to be effective to refine the microstructure of the ingots. Figure 5b shows the typical microstructure of the ingots prepared at intermediate cooling rate of 0.278 $\mathrm{K \cdot s^{-1}}$. The microstructure consists of three types of grains: (i) lamellar $\alpha_2 + \gamma$, (ii) γ and (iii) remaining β(B2) and/or transformed ω. The mean grain size is measured to be 21 μm. Similar microstructure is observed after cooling at 0.056 $\mathrm{K \cdot s^{-1}}$, as seen in Fig. 5c. However, this lowest cooling rate results in a coarser mean grain size of 32 μm. Figure 6 shows the microstructure in the vicinity of the grain boundaries. The size of β(B2), ω (cannot be distinguished from β by SEM) and γ grains is smaller in the ingots prepared at the

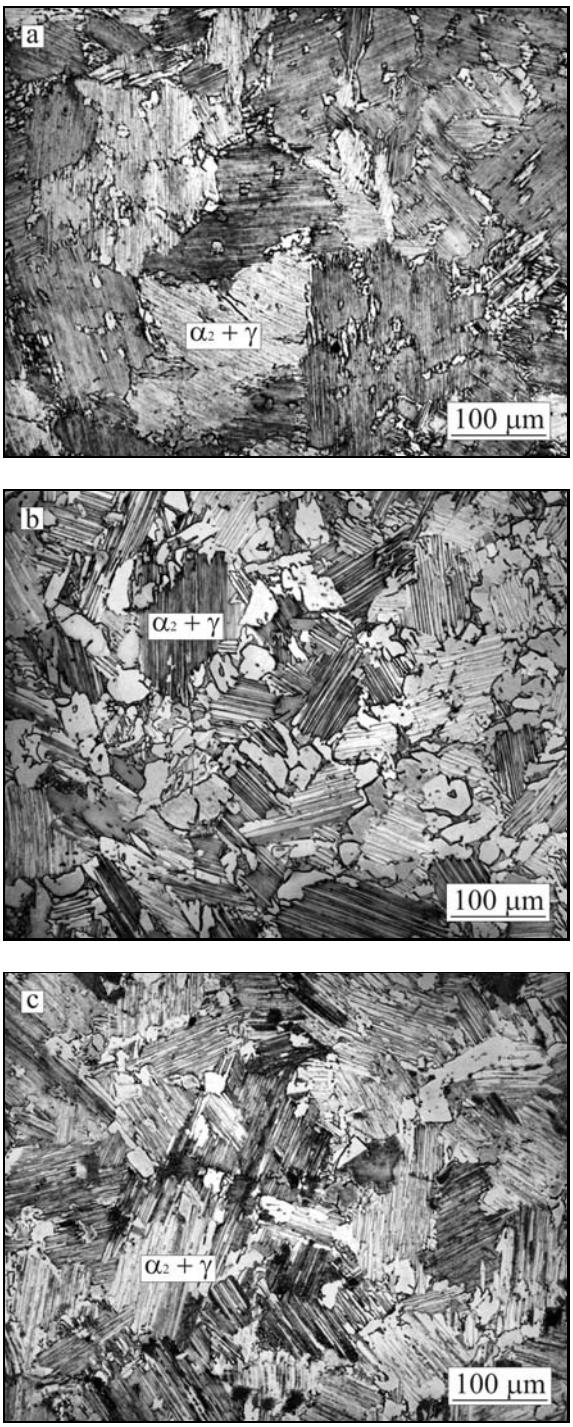

Fig. 5. LOM micrographs showing the effect of cooling rate on the microstructure of the ingots annealed at 1623 K for 600 s. Cooling rates: (a) 1.181 $K \cdot s^{-1}$; (b) 0.278 $K \cdot s^{-1}$; (c) 0.056 $K \cdot s^{-1}$.

highest cooling rate of 1.181 $K \cdot s^{-1}$ (Fig. 6a) when compared to that in ingot prepared at the lowest cooling rate of 0.056 $K \cdot s^{-1}$ (Fig. 6b). In addition, the microstructures contain needle- and ribbon-like boride particles in the vicinity of grain boundaries, which effectively constrain the grain growth during heat treatments.

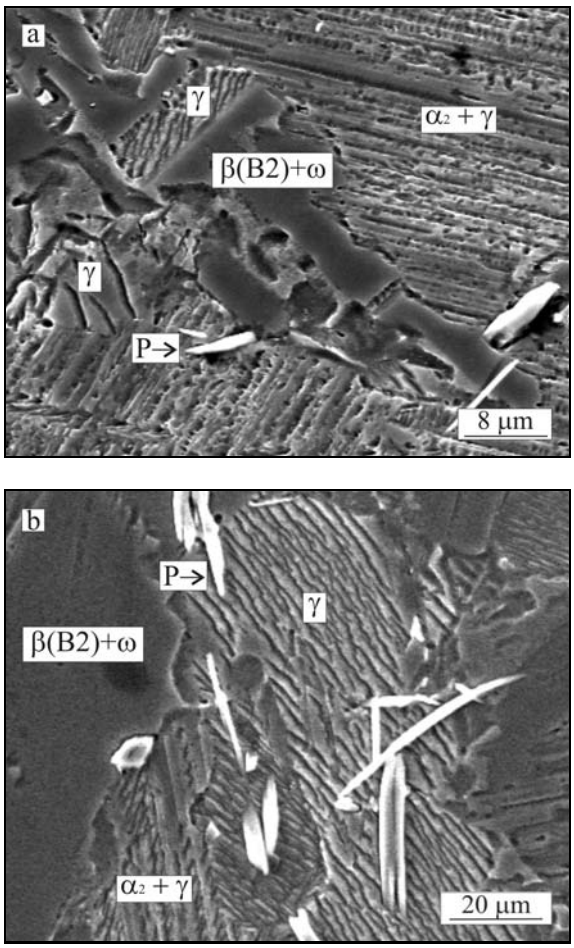

Fig. 6. SEM micrographs showing the effect of cooling rate on the microstructure in the vicinity of the grain boundaries of the ingots annealed at 1623 K for 600 s. Cooling rates: (a) 1.181 $K \cdot s^{-1}$; (b) 0.056 $K \cdot s^{-1}$. P – boride particles.

Figure 7 shows dependence of mean interlamellar α_2-α_2 spacing determined from log-normal distribution curves on the cooling rate. The calculated mean values of interlamellar spacing λ decrease with increasing cooling rate $\dot{\nu}$ according to relationship

$$\lambda = K\dot{\nu}^a, \tag{1}$$

where K is a material constant and a is the cooling rate exponent. Using regression analysis, the cooling rate exponent was determined to be $a = -0.14 \pm 0.01$. This value is significantly higher than that of -0.46 measured in Ti-46Al-2W-0.5Si (at.%) alloy [28]. This discrepancy can be related to different growth kinetics of γ lamellae from the α phase resulting from different alloying additions and especially from a lower content of aluminium in the studied alloy, which probably affects the etched lamellar structure (Fig. 6) subjected to quantitative metallographic evaluation.

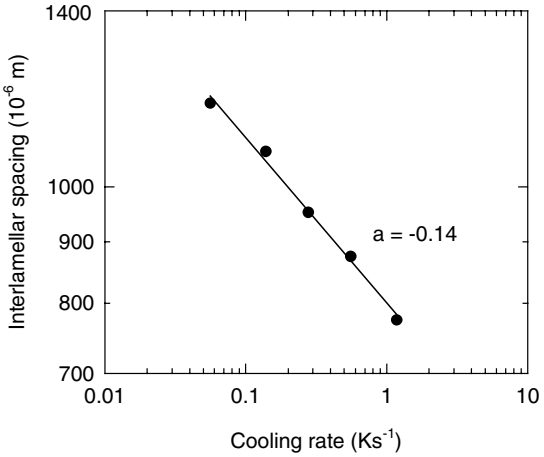

Fig. 7. Dependence of mean interlamellar α_2-α_2 spacing on the cooling rate.

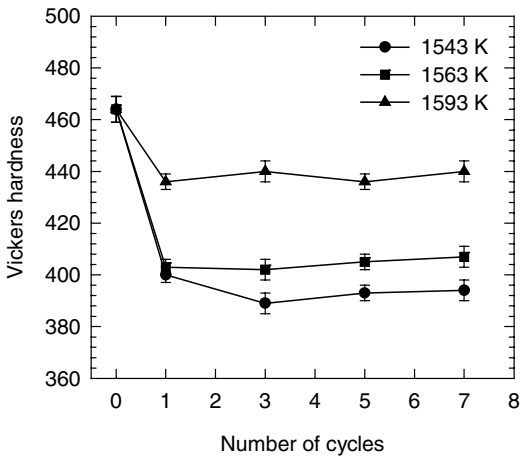

Fig. 8. Dependence of Vickers hardness on the number of heat treatment cycles. The annealing temperatures are indicated in the figure.

3.2. Mechanical properties

3.2.1. Effect of cyclic heat treatments on mechanical properties

Figure 8 shows dependence of Vickers hardness on the number of applied cycles after oil quenching from three annealing temperatures of 1543, 1563 and 1593 K and stabilization annealing at 1173 K for 6 h. The hardness decreases after the first applied cycle and increasing number of the cycles has no statistical effect on the hardness values. Decrease of annealing temperature leads to a decrease of Vickers hardness.

Room-temperature tensile tests revealed that all specimens subjected to cyclic heat treatments are very brittle and show tensile fracture at ultimate tensile stresses (UTS) ranging from about 500 to

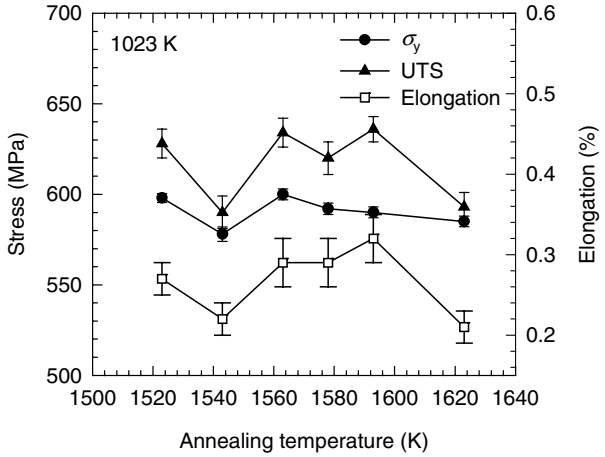

Fig. 9. Variation of high-temperature offset tensile yield stress (σ_y), ultimate tensile stress (UTS) and plastic elongation to fracture at 1023 K with the annealing temperature of the cyclic heat treatment.

550 MPa. Since the measured plastic deformations to fracture were inferior to 0.08 %, 0.2 % offset yield stresses could not be determined from the tensile stress-strain curves. Figure 9 summarizes the results of high-temperature tensile tests at 1023 K. The tensile specimens (5 specimens for each regime) were subjected to 3 heat treatment cycles consisting of annealing at 6 temperatures ranging from 1523 to 1623 K for 600 s, quenching into the oil and stabilization annealing at 1173 K for 6 h. The 0.2 % offset yield stress (σ_y) is measured to vary from 578 to 600 MPa, ultimate tensile stress (UTS) from 590 to 636 MPa and the plastic elongation to fracture from 0.21 to 0.32 %. However, no clear effect of the annealing temperature or resulting microstructure on the high-temperature tensile properties can be identified. Such variations in mechanical properties are quite typical for cast TiAl-based aluminides [29].

3.2.2. Effect of cooling rate on mechanical properties

Figure 10 shows dependence of Vickers hardness on the cooling rate for the specimens annealed at 1623 K for 600 s and then cooled at constant cooling rates ranging from 0.056 to 1.181 $K \cdot s^{-1}$ to a temperature of 1073 K. Vickers hardness increases from HV = 340 with increasing cooling rate and reaches a maximum value of HV = 394 after cooling at a rate of 1.181 $K \cdot s^{-1}$. Figure 11 summarizes the results of room-temperature compression tests. As seen in this figure, the 0.2 % offset compressive yield stress increases and both ultimate compressive stress and plastic deformation to fracture decrease with increasing cooling rate. As illustrated in Figs. 10 and 11, both the hardness and compressive yield stress show similar evolution with the increasing cooling rate. Hence, a functional

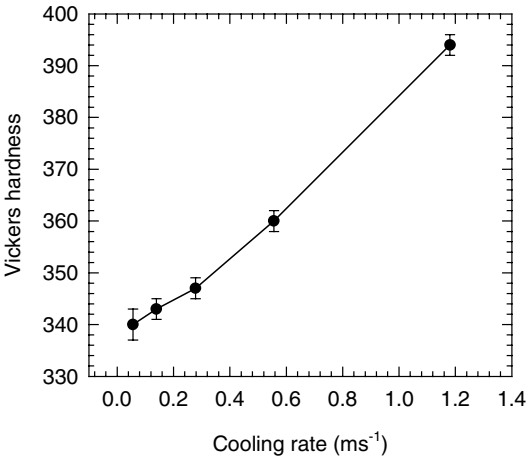

Fig. 10. Dependence of Vickers hardness on the cooling rate.

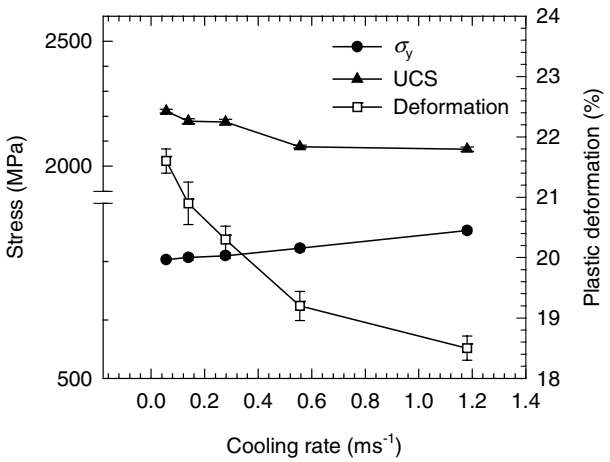

Fig. 11. Variation of room-temperature offset compressive yield stress (σ_y), ultimate compressive stress (UCS) and plastic deformation to fracture on the cooling rate.

dependence between these two parameters might be determined, as shown previously by several authors [30–32]. Figure 12 shows variation of the compressive yield stress with the Vickers hardness. The yield stress σ_y increases linearly with increasing Vickers hardness HV according to relationship

$$\sigma_y = K_0 + K_1 \mathrm{HV}, \tag{2}$$

where K_0 and K_1 are the material constants. Linear regression analysis of the experimental data yields an equation for the yield stress in the form

$$\sigma_y = 392.9 + 0.91\mathrm{HV}. \tag{3}$$

The correlation coefficient of this fit is $r^2 = 0.98$.

As shown recently by several authors [28, 33, 34] for

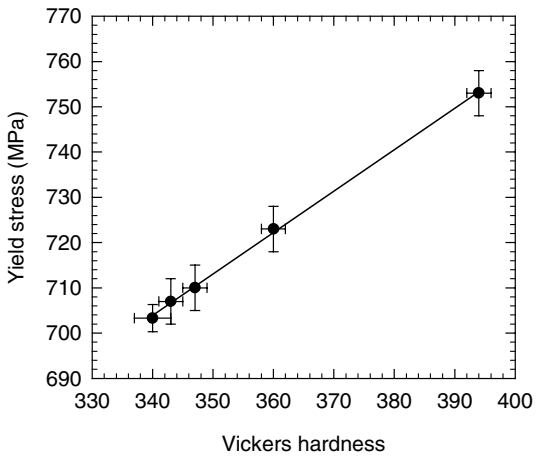

Fig. 12. Linear dependence of room-temperature compressive yield stress on the Vickers hardness.

TiAl-based alloys with fully lamellar structure, the increase of hardness and compressive yield stress is proportional to an inverse value of square root of mean interlamellar α_2-α_y spacing λ according to a Hall-Petch type relationship in the form

$$\sigma_y = \sigma_o + k_y \frac{1}{\sqrt{\lambda}}, \tag{4}$$

where σ_o is the stress corresponding to the lattice resistance to dislocation slip in the γ-phase and k_y is a parameter which is related to the critical stress necessary to generate dislocation in the α_2 lamella. It is of interest to investigate whether such relationship is still valid for complex microstructure of the studied alloy, which contains not only fully lamellar $\alpha_2 + \gamma$ grains but numerous equiaxed β(B2), γ and ω grains. Figure 13 shows dependence of compressive yield stress and Vickers hardness on an inverse value of square root of mean interlamellar α_2-α_2 spacing λ. It is clear that the experimental results deviate significantly from a straight line predicted from Eq. (4) and cubic regression equation instead linear one should be used to fit the data. The parameter k_y is measured to increase continuously from 0.05 at a cooling rate of 0.056 $\mathrm{K \cdot s^{-1}}$ to 0.65 $\mathrm{MPa \cdot m^{0.5}}$ at 1.181 $\mathrm{K \cdot s^{-1}}$. Constant values of 0.18 and 0.22 $\mathrm{MPa \cdot m^{0.5}}$ were reported for fully lamellar Ti-46Al-2W-0.5Si (at.%) alloy with two different orientations of $\alpha_2 + \gamma$ lamellae to the loading axis [28].

All tensile specimens tested at room temperature were brittle and showed very limited plastic deformation to fracture (below 0.1 %). Figure 14 summarizes the results of room temperature tensile tests. Maximum and minimum value of UTS of 568 and 435 MPa are measured after cooling at rates of 0.139 and 0.278 $\mathrm{K \cdot s^{-1}}$, respectively. Figure 15 shows fracture surfaces after room-temperature tensile tests. The typical brittle translamellar fracture mode is evident for

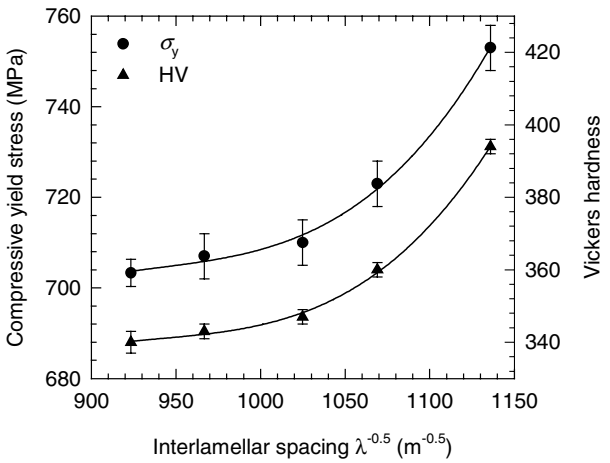

Fig. 13. Dependence of room-temperature compressive yield stress (σ_y) and Vickers hardness on inverse value of square root of mean interlamellar α_2-α_y spacing λ.

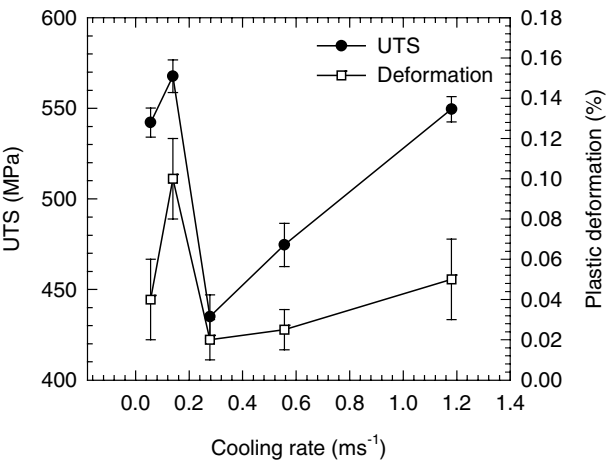

Fig. 14. Variation of room-temperature ultimate tensile stress (UTS) and plastic elongation to fracture on the cooling rate.

this type of material. Some cracks indicate delamination along lamellar interfaces perpendicular to fracture surface, as seen in Fig. 15a. Larger cracks are observed along the grain boundaries. It should be noted that the as-cast ingot contained casting defects such as porosity and bubbles. In spite of the fact that each ingot and tensile specimen was carefully checked before the heat treatments and machining, some tensile specimens showed premature fracture without yielding at relatively low stresses. Fractographic analysis revealed that these specimens contain casting defects, as shown in Fig. 15b. The results of the tensile tests on the specimens containing such evident casting defects were considered to be not valid and new ingots were prepared to maintain 5 tensile specimens for each heat treatment regime.

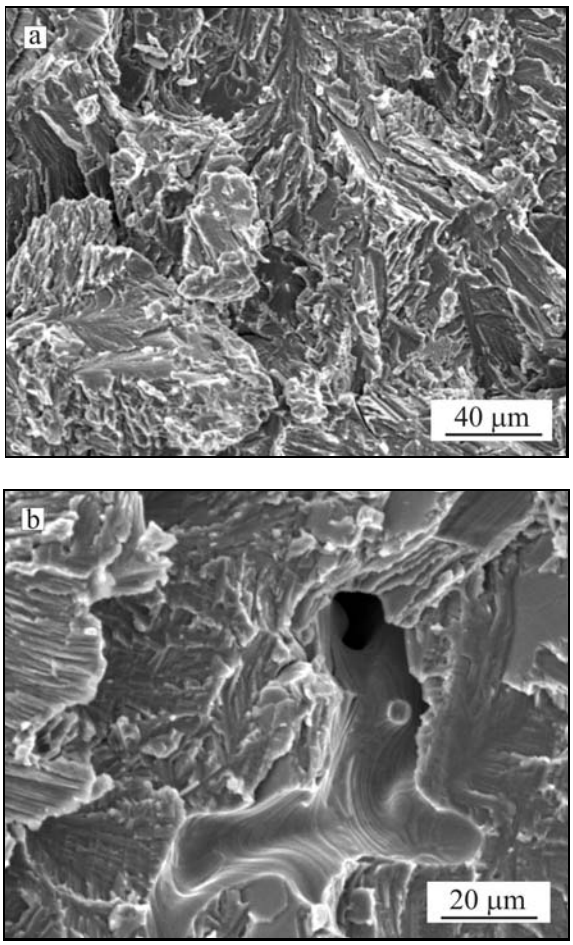

Fig. 15. SEM micrographs showing the typical features of room-temperature tensile fracture: (a) brittle translamellar fracture; (b) casting porosity on the fracture surface.

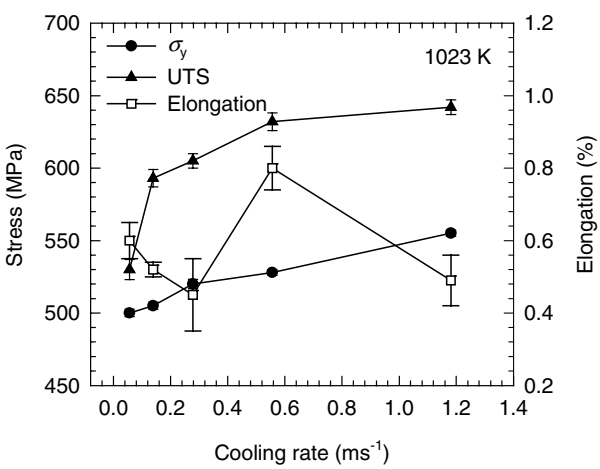

Fig. 16. Variation of high-temperature offset tensile yield stress (σ_y), ultimate tensile stress (UTS) and plastic elongation to fracture at 1023 K on the cooling rate.

Figure 16 summarizes the results of high-temperature tensile tests at 1023 K. Both the 0.2 % offset tensile

yield stress and UTS increase with increasing cooling rate. The plastic elongation to fracture varies from 0.45 to 0.8 % without any definite dependence on the cooling rate. This heat treatment leads to a higher plastic elongation to fracture (from 0.45 to 0.8 %) but lower yield stresses (from 500 to 555 MPa) than those measured for specimens after cyclic heat treatments.

4. Conclusions

The investigation of the effect of heat treatments on the microstructure and mechanical properties of a cast Ti-44Al-4Nb-4Zr-0.2Si-0.3B (at.%) alloy suggests the following conclusions:

1. The microstructure of cast Ti-44Al-4Nb-4Zr-0.2Si-0.3B (at.%) ingots subjected to cyclic heat treatment and heat treatment combined with cooling at various constant cooling rates consists of equiaxed β(B2), γ, ω and lamellar $\alpha_2 + \gamma$ grains.

2. Decrease of annealing temperature from 1593 to 1543 K leads to a significant decrease of mean grain size during the cyclic heat treatments. The grain size is decreased after the first cycle. Increasing number of the cycles has no statistical effect on the grain size.

3. Increase of cooling rate leads to a decrease of interlamellar α_2-α_2 spacing within lamellar $\alpha_2+\gamma$ grains and formation of numerous equiaxed γ, β(B2) and ω grains in the microstructure. The mean interlamellar α_2-α_2 spacing λ decreases with increasing cooling rate $\dot{\nu}$ according to relationship $\lambda \propto \dot{\nu}^a$, where cooling rate exponent is determined to be $a = -0.14$.

4. Decrease of annealing temperature from 1593 to 1543 K leads to a decrease of Vickers hardness during the cyclic heat treatments. A significant decrease of the hardness is achieved after the first cycle. The cyclic heat treatment does not improve room temperature ductility of the studied alloy. Tensile specimens tested at 1023 K showed clear yielding with well defined 0.2 % offset tensile yield stress and total plastic elongation to fracture ranging from 0.21 to 0.32 %.

5. Increase of cooling rate increases Vickers hardness, room-temperature 0.2 % offset compressive yield stress, high-temperature 0.2 % offset tensile yield stress and high-temperature ultimate tensile stress. Heat treatment with cooling at constant cooling rates does not improve room-temperature ductility. Tensile specimens tested at 1023 K showed clear yielding and total plastic elongation to fracture ranging from 0.45 to 0.8 %.

Acknowledgements

The authors gratefully acknowledge the financial support of the Slovak Grant Agency for Science under the contract VEGA 2/4166/24.

References

[1] DIMIDUK, D. M.: Mater. Sci. Eng. A, *263*, 1999, p. 281.
[2] TETSUI, T.: Mater. Sci. Eng. A, *329–331*, 2002, p. 582.
[3] NAZMY, M.—LUPINC, V.: In: Materials for Advanced Power Engineering 2002. Eds.: Lecomte-Beckers, J., Carton, J. M., Schubert, F., Ennis P. J. Vol. 21. Part I. Jülich, Forschungszentrum Jülich GmbH 2002, p. 43.
[4] LAPIN, J.—PELACHOVÁ, T.: Kovove Mater., *42*, 2004, p. 143.
[5] LAPIN, J.: Kovove Mater., *43*, 2005, p. 81.
[6] ORLOVÁ, A.—KUCHAŘOVÁ, K.—DLOUHÝ, A.: Kovove Mater., *43*, 2005, p. 55.
[7] LUKÁŠ, P.—ČADEK, J.—KUNZ, L.—SVOBODA, M.—KLUSÁK, J.: Kovove Mater., *43*, 2005, p. 5.
[8] MALDINI, M.—LUPINC, V.—ANGELLA, G.: Kovove Mater., *42*, 2004, p. 283.
[9] MALDINI, M.—LUPINC, V.—ANGELLA, G.: Kovove Mater., *42*, 2004, p. 21.
[10] VAŇO, A.—PELACHOVÁ, T.: Kovove Mater., *42*, 2004, p. 121.
[11] LAPIN, J.—BAJANA, O.: Kovove Mater., *43*, 2005, p. 169.
[12] LAPIN, J.: Intermetallics, *14*, 2006, p. 1417.
[13] PRAHL, J.—HAUŠILD, P.—KARLÍK, M.—CRENN, J. F.: Kovove Mater., *43*, 2005, p. 134.
[14] KRATOCHVÍL, P.—HANUS, P.—HAKL, J.—VLASÁK, T.: Kovove Mater., *42*, 2004, p. 73.
[15] HAUŠILD, P.—KARLÍK, M.—NEDBAL, I.—PRAHL, J.: Kovove Mater., *42*, 2004, p. 156.
[16] VOJTĚCH, D.—ČÍŽOVÁ, H.—MAIXNER, J.: Kovove Mater., *43*, 2005, p. 317.
[17] LEYENS, C.—PETERS, M.: Titanium and Titanium Alloys – Fundamentals and Applications. Weinheim, Wiley-VCH Verlag GmbH & Co. KGaA 2005.
[18] HARDING, R. A.: Kovove Mater., *42*, 2004, p. 225.
[19] BOHN, R.—KLASSEN, T.—BORMANN, R.: Acta Mater., *49*, 2001, p. 299.
[20] CHENG, T. T.: Intermetallics, *8*, 2000, p. 29.
[21] CHENG, T. T.—WILLIS, M. R.—JONES, I. P.: Intermetallics, *7*, 1999, p. 89.
[22] CHENG, T. T.: Intermetallics, *8*, 2000, p. 29.
[23] MAZIASZ, P. J.—RAMANUJAN, R. V.—LIU, C. T.—WRIGHT, J. L.: Intermetallics, *5*, 1997, p. 83.
[24] ZANG, W. J.—DEVI, S. C: Mater. Sci. Eng. A, *337*, 2002, p. 17.
[25] CHENG, T. T.—WILLIS, M. R.: Scripta Mater., *39*, 1998, p. 1255.
[26] CHENG, T. T.—LORETTO, M. H.: Acta Mater., *46*, 1998, p. 4801.
[27] WANG, J. N.—YANG, J.—XIA, Q.—WANG, Y.: Mater. Sci. Eng. A, *329–331*, 2002, p. 118.
[28] LAPIN, J.—ONDRÚŠ, Ľ.—BAJANA, O.: Mater. Sci. Eng. A, *360*, 2003, p. 85.
[29] MI, J.—HARDING, R. A.—CAMPBELL, J.: Metall. Mater. Trans. A, *35A*, 2004, p. 2893.
[30] LAPIN, J.—ONDRÚŠ, Ľ.—NAZMY, M.: Intermetallics, *10*, 2002, p. 1019.
[31] MUÑOZ-MORRIS, M. A.—FERNÁNDEZ, I. G.—MORRIS, D. G.: Scripta Mater., *46*, 2002, p. 617.

[32] GIL, I.—MUÑOZ-MORRIS, M. A.—MORRIS, D. G.: Intermetallics, *9*, 2001, p. 373.
[33] LAPIN, J.: J. Mater. Sci. Lett., *22*, 2003, p. 747.
[34] KISHIDA, K.—JOHNSON, D. R.—MASUDA, Y.—UMEDA, H.—INUI, H.—YAMAGUCHI, M.: Intermetallics, *6*, 1998, p. 679.